Research Square

Preprints are preliminary reports that have not undergone peer review.
They should not be considered conclusive, used to inform clinical practice,
or referenced by the media as validated information.

Density-dependent HPGe efficiency from multi-gamma line ratios: a nominal-plus-self-shielding method and its MATLAB implementation

Steven R. Biegalski

sbiegalski6@gatech.edu

Georgia Institute of Technology

Research Article

Keywords: Gamma-ray spectrometry, Self-attenuation, Full-energy peak efficiency, Monte Carlo, Nuclear forensics, Post-detonation debris

Posted Date: November 10th, 2026

DOI: https://doi.org/10.21203/rs.3.rs-11501660/v1

License: This work is licensed under a Creative Commons Attribution 4.0 International License.
Read Full License

Additional Declarations: No competing interests reported.

Density-dependent HPGe efficiency from multi-gamma line ratios: a nominal-plus-self-shielding method and its MATLAB implementation

Steven R. Biegalski*

Nuclear and Radiological Engineering Program, George W. Woodruff School of Mechanical Engineering, Georgia Institute of Technology, 770 State Street, Atlanta, GA 30332, USA

**Corresponding author: sbiegalski6@gatech.edu*

Abstract

Gamma-ray self-attenuation in dense samples biases activities measured with a germanium detector. This method infers an effective sample density from the spectrum itself, using the relative intensities of several lines from each multi-gamma nuclide and a Monte Carlo efficiency that is a function of energy (keV) and sample density (g cm^{-3}). Only the density dependence of the surface is applied to the laboratory calibration, so systematic errors in the detector model are largely removed. A MATLAB code automates peak search, identification, density fitting, uncertainty propagation and activity correction. In synthetic tests from 1.5 to 20 g cm^{-3} the fitted density was within 0.3 g cm^{-3} of the anticipated value.

Keywords

Gamma-ray spectrometry · Self-attenuation · Full-energy peak efficiency · Monte Carlo · Nuclear forensics · Post-detonation debris

Introduction

A full-energy peak efficiency curve for a high-purity germanium (HPGe) detector is normally measured with a mixed-nuclide standard whose matrix is water, epoxy or some other material of density near 1 g cm^{-3}. The curve is then applied to samples counted in the same container and position. That transfer is safe when the sample resembles the standard, as it does in routine neutron activation analysis of filters and biological materials [1]. It fails when the sample is much denser, because photons emitted inside the sample are attenuated on their way to the crystal, and the loss is largest at low energy where the attenuation coefficients climb steeply [2, 3]. The result is an activity that is too low and an apparent efficiency curve that bends downward at low energy in a way that the calibration does not predict.

The classical correction is the transmission method. This method utilizes collimated beam from an external point source to measure the transmission amd provide a linear attenuation coefficient. This attenuation coefficient may then be utilized to calculate a self-absorption factor. Cutshall *et al*. introduced this approach for the 46.5 keV line of ^{210}Pb in sediments [4]. Jodłowski identified issues with this method including sample-to-sample inhomogenity that was significant enough to require a revision factor [5].

Post-detonation debris is a hard case for any of these approaches. Debris from a nuclear explosion in a city will be fused and mixed with building materials, glass, soil and metal, so samples will vary in density and composition and will rarely be shaped to match a calibration standard [6, 7]. Rapid and defensible gamma spectrometry of such material is a core need of the nuclear forensics mission [7], and radionuclide observables from historic tests show how much interpretation rests on accurate activity ratios [8]. To support method development, surrogate post-detonation urban debris (SPUD) materials were produced as candidate standard reference materials and characterized by neutron activation and gamma spectrometry [9], using characterized irradiation facilities at The University of Texas at Austin TRIGA Reactor [10, 11].

An alternative to transmission measurements is to model the counting geometry by Monte Carlo [12]. The full-energy peak efficiency of the detector may be computed with MCNP6.1 [13] for a cylindrical carbon source whose density is varied from 1 to 21 g cm^{-3}. The detector efficiency may be fit as a polynomial surface in density and log energy. The density of an unknown sample can then be found from the ratio of the count rates of two lines of one nuclide, because in that ratio the unknown activity cancels. With the density in hand, the surface gives the efficiency at every energy.

The method is implemented in a MATLAB code titled SSEff (self-shielding efficiency). SSEff implements four new strategies. First, the efficiency is written as the product of the laboratory's own nominal calibration and a self-shielding correction taken from the MCNP surface, so that only the density dependence of the model is transferred. Detector-specific errors in the Monte Carlo description cancel to first order. Second, instead of one line pair, all usable lines of all identified multi-gamma nuclides enter a single least-squares fit for the effective density, with the nuclide activities eliminated analytically, and the uncertainties of the peak areas, the nominal calibration and the surface model are propagated, with their correlations, into the corrected efficiency curve. Third, the whole chain from spectrum file to corrected efficiency curve and activities is automated, with peak search, peak fitting, nuclide identification and a graphical interface. Fourth, any inconsistency in the original listing of the two-line density script is identified and corrected, which brings its worked example back into agreement with the comparison data. The reporting within this manuscript utilize quantitative tests utilizing synthetic spectra with the implications discussed in the final section.

Theory

Efficiency surface

The MCNP6.1 model represents the ORTEC coaxial HPGe detector used for the SPUD measurements, including dead layers, contacts and the aluminum end cap, with the F8 pulse-height tally in the active germanium. Monte Carlo transport is preferred over deterministic methods [14] because the geometry and the energy-dependent interactions

can be represented directly. The source is a uniform carbon cylinder 2.28 cm in diameter and 1.2 cm high inside a polyethylene vial, with its center about 12 cm above the front of the crystal. Trials with real materials of increasing density (from HCl to Pu) produce surfaces with K-edge structure and crossing efficiency curves, so the matrix is fixed as carbon ($Z = 6$) and only its density is varied. With a large number of histories and without the 50 keV line, the fit used here is

$$ln\,\varepsilon(E,\rho) = f(\rho,y) = \sum_{i=0}^{3}\sum_{j=0}^{4-i} p_{ij}\rho^i y^j\,, \qquad y = ln(E/\text{keV}) \tag{1}$$

which is MATLAB's poly34 form. The equation is a function of density ρ (g cm^{-3}) and energy (keV). The equation is nominally valid from 67.75 to 2754 keV and from 1 to 21 g cm^{-3}. The efficiency fit is not valid at low energies due to sample K-edge effects mentioned previously. The coefficients must be carried at full precision as density is raised to up to the the third power.

Two-line density

For a line of energy E_j and emission probability I_j from a nuclide of activity a, the net peak area is $A_j = a\,t\,I_j\,\varepsilon(E_j)$, so the ratio of two lines of the same nuclide does not depend on the activity:

$$R = \frac{\frac{A_1}{I_1}}{\frac{A_2}{I_2}} = \frac{\varepsilon(E_1,\rho)}{\varepsilon(E_2,\rho)} = exp[f(\rho,y_1) - f(\rho,y_2)] \tag{2}$$

Because f is cubic in ρ, the condition ln $R = f(\rho, y_1) - f(\rho, y_2)$ is a cubic equation in density whose coefficients are fixed by the two energies. It is solved with MATLAB's roots function, and the physical root is selected.

Nominal efficiency with a self-shielding correction

Equation 2 treats the MCNP surface as the absolute efficiency of the detector. Any difference between the modeled and the real detector (crystal dimensions, dead layer, distance) then enters the density estimate directly, and the difference can easily be several percent with an energy-dependent shape. Most laboratories already hold a measured calibration $\varepsilon_{nom}(E)$ obtained with a standard of known density ρ_{cal} in the sample geometry. SSEff keeps that calibration and borrows only the change in efficiency with density from the surface:

$$ln\,\varepsilon(E,\rho) = ln\,\varepsilon_{\mathrm{nom}}(E) + f(\rho, ln\,E) - f(\rho_{\mathrm{cal}}, ln\,E) \tag{3}$$

The self-shielding correction factor relative to the calibration standard is then

$$\mathrm{CF}(E,\rho) = \frac{\varepsilon(E,\rho)}{\varepsilon_{\mathrm{nom}}(E)} = exp[f(\rho, ln\,E) - f(\rho_{\mathrm{cal}}, ln\,E)] \tag{4}$$

with CF = 1 at $\rho = \rho_{cal}$. A Monte Carlo model may be poor in absolute terms and still good in ratio, because errors in the detector description affect the calibration geometry and the sample geometry in nearly the same way. If the nominal efficiency is taken to be the surface itself at ρ_{cal}, Eq. 3 reduces to $\exp[f(\rho, \ln E)]$, the absolute surface method. The code supports three nominal options: the surface at ρ_{cal}, a table of measured calibration points fitted with a weighted polynomial in $\ln \varepsilon$ versus $\ln E$, or polynomial coefficients entered directly in the form used by Genie 2000 [15]. The default is $\rho_{cal} = 1.0$ g/cm^3.

With Eq. 3 the two-line condition becomes

$$\Delta f(\rho) = ln\,R - \Delta\, ln\,\varepsilon_{\mathrm{nom}} + \Delta f(\rho_{\mathrm{cal}}) \tag{5}$$

Here, $\Delta f(\rho) = f(\rho, y_1) - f(\rho, y_2)$. The left side is still $\sum_i \rho^i \sum_j p_{ij}(y_1^j - y_2^j)$, so the equation remains a cubic in ρ with a modified constant term. SSEff solves it for every line pair of

every identified nuclide and keeps the root inside [1, 21] g cm^{-3}. If σ(ln R) is the standard uncertainty of the log ratio, the density uncertainty of a pair is

$$\sigma_\rho = \frac{\sigma(\ln R)}{|\partial \Delta f / \partial \rho|} \tag{6}$$

where Δf is the left side of Eq. 5. The derivative is the sensitivity of the pair, and it varies by an order of magnitude between pairs, as shown below.

Global multi-line fit

A single pair discards most of the information in a spectrum that may contain twenty or more usable lines from several nuclides. For line j belonging to nuclide n define the apparent log efficiency

$$y_j = \ln\left(\frac{A_j}{I_j}\right) = c_n + \ln \varepsilon(E_j, \rho) \tag{7}$$

where $c_n = \ln(a_n\ t_{live}/C_{d,n})$ collects the unknown activity, the live time and the decay correction of nuclide n. For a trial density, the best c_n is the weighted mean of $y_j - \ln \varepsilon(E_j, \rho)$ over the lines of that nuclide, and the remaining misfit is

$$\chi^2(\rho) = \sum_j w_j \left[y_j - c_n(\rho) - \ln \varepsilon(E_j, \rho)\right]^2, \qquad c_n(\rho) = \frac{\sum_{j \in n} w_j \left[y_j - \ln \varepsilon(E_j, \rho)\right]}{\sum_{j \in n} w_j} \tag{8}$$

This profile χ^2 depends on ρ alone and is minimized on [1, 21] g/cm^3, first on a 401-point grid and then by a bounded one-dimensional search. Each nuclide only constrains the shape of the efficiency curve across its own lines, and the scale is free, so the fit uses exactly the information exploited by the two-line ratio, but for all pairs at once and with proper weighting. The weights are

$$\frac{1}{w_j} = \left(\frac{\sigma_{A,j}}{A_j}\right)^2 + \left(\frac{\sigma_{I,j}}{I_j}\right)^2 + u_{\mathrm{m}}^2 \tag{9}$$

combining the relative uncertainties of the peak area and of the emission probability with a relative uncertainty u_{m} assigned to the surface model. The default $u_{\mathrm{m}} = 2\%$ follows the comparison of the surface with independent MCNP data. With N lines from K nuclides the number of degrees of freedom is $\nu = N - K - 1$. The density uncertainty is the half-width of the interval in which χ^2 rises by one above its minimum, multiplied by the Birge ratio $(\chi^2/\nu)^{1/2}$ when that ratio exceeds one [16]. A fit that ends on the search boundary is flagged, since it usually means the model does not describe the data.

Activities

Once ρ_{eff} is known, each line gives an activity

$$a_j = \frac{n_j C_{\mathrm{d}}}{I_j \varepsilon\left(E_j, \rho_{\mathrm{eff}}\right) t_{\mathrm{live}}}, \qquad C_{\mathrm{d}} = \frac{\lambda t_{\mathrm{real}}}{1 - e^{-\lambda t_{\mathrm{real}}}} \tag{10}$$

where n_{j} is the net area and C_{d} corrects for decay during the count, so that a_{j} refers to the start of acquisition. The activity a_{n} of nuclide n is the inverse-variance weighted mean of its line activities:

$$a_n = \frac{\sum_{j \in n} w_j a_j}{\sum_{j \in n} w_j}, \qquad \sigma(a_n) = \left(\sum_{j \in n} w_j\right)^{-1/2}, \qquad w_j = \frac{1}{\sigma\left(a_j\right)^2} \tag{11}$$

SSEff computes Eq. 11 twice, with the nominal efficiency and with the corrected one, and adds the density uncertainty to the corrected result through the weighted mean of $\partial \ln \varepsilon / \partial \rho$ over the lines. The reduced χ^2 of the line activities about their mean is reported for both. It is a useful diagnostic in its own right: when self-shielding is present and ignored,

low-energy lines give lower activities than high-energy lines of the same nuclide and the scatter is far larger than the uncertainties allow.

Propagation of uncertainty

Three groups of inputs carry uncertainty into the corrected efficiency: 1) the peak areas and emission probabilities, 2) the surface model, represented by the relative uncertainty u_m and 3) the nominal calibration. When the nominal efficiency is fitted to calibration points, the coefficient vector $\mathbf{a}$ of the polynomial in ln E has the weighted least-squares covariance $\mathbf{C}_a = (\mathbf{A}^T\mathbf{W}\mathbf{A})^{-1}$. The calibration also affects the fitted density, because ρ_{eff} responds to the shape of $\varepsilon_{nom}(E)$ across the lines. The sensitivity $\mathbf{g} = \partial\rho_{eff}/\partial\mathbf{a}$ is obtained numerically by repeating the density fit with $\mathbf{a}$ displaced by plus and minus one standard deviation along each principal axis of $\mathbf{C}_a$, so that every displaced calibration is a physically plausible curve. To first order,

$$\sigma^2(\rho_{eff}) = \sigma_{fit}^2 + \boldsymbol{g}^T\boldsymbol{C}_a\boldsymbol{g},\ \mathrm{cov}[ln\,\varepsilon_{nom}(E)\,,\rho_{eff}] = \boldsymbol{v}(E)^T\boldsymbol{C}_a\boldsymbol{g} \qquad (12)$$

where $\mathbf{v}(E) = (1,\ \ln E,\ (\ln E)^2,\ \ldots)^T$. With $d(E) = \partial f(\rho,\ \ln E)/\partial\rho$ evaluated at ρ_{eff}, the variance of the logarithm of the corrected efficiency of Eq. 3 is

$$u^2(E) = \mathrm{var}[ln\,\varepsilon_{nom}(E)] + d(E)^2\sigma^2(\rho_{eff}) + 2d(E)\mathrm{cov}[ln\,\varepsilon_{nom}(E)\,,\rho_{eff}] + u_m^2 \qquad (13)$$

and $u(E)$ is the relative standard uncertainty of $\varepsilon(E,\ \rho_{eff})$. A calibration that is too high at low energy relative to high energy pushes the fitted density up, which lowers the correction factor at low energy, so the two errors partly cancel in the corrected curve. For the self-shielding factor alone the uncertainty is

$$u_{CF}(E) = [d(E)^2\sigma^2(\rho_{eff}) + u_m^2]^{1/2} \qquad (14)$$

A relative calibration uncertainty that is the same at all energies, such as the activity uncertainty of the standard, cancels in the density fit and enters Eq. 13 only through the

first term. In the activities of Eq. 11 the calibration and density terms are common to all lines of a nuclide, so they are added in quadrature after averaging rather than to the individual line weights. SSEff reports each term of Eq. 13 as a function of energy along with the corrected curve.

Implementation

Input and peak analysis

SSEff is written in MATLAB (developed with R2024b) and can be used through functions or a graphical interface. It reads ORTEC SPE and CHN files and two-column CSV or text spectra; Canberra CNF files are read after export with the vendor's conversion utility. A peak list from another program (energy, net area and uncertainty, for example a Genie 2000 report) can be imported instead of a spectrum, in which case the peak search is skipped.

Peaks are located with a smoothed second-difference filter of the Mariscotti type [17] similar to the second-difference search in Genie 2000 [15]. The spectrum is folded with a zero-area kernel shaped as the negative second derivative of a Gaussian whose width follows the local resolution, so that a linear background cancels, and channels at which the filter output exceeds four standard deviations of its own counting noise become candidates. Candidates closer than 0.6 FWHM are merged. Peaks whose fitting regions overlap are grouped, and each group is fitted with Gaussians on a linear background. Centroids and a common width scale are nonlinear parameters and the amplitudes and background are solved linearly inside the objective. Weights start as Neyman weights and are iterated with the fitted model (Pearson weights), which removes the familiar low-count bias of Neyman weighting. Area uncertainties come from the full covariance matrix of a numerical Jacobian, so the correlation between area and width is included, and they are inflated by the reduced χ^2 of the fit when that exceeds one. A sum-method area with side-band background is also reported for isolated peaks. The resolution model $\mathrm{FWHM} = (a + bE)^{-1/2}$ is refitted from strong isolated peaks and the search is repeated with the refined widths.

Nuclide library and identification

The library contains 40 nuclides and 386 gamma lines taken from ENSDF evaluations through NuDat 3.0 [18]. It covers common calibration nuclides (^{57}Co, ^{60}Co, ^{75}Se, ^{88}Y, ^{124}Sb, ^{125}Sb, ^{133}Ba, ^{134}Cs, ^{152}Eu, ^{154}Eu and ^{192}Ir), the activation and fission products reported in the SPUD measurements [9], such as ^{24}Na, ^{27}Mg, ^{56}Mn, ^{46}Sc, ^{59}Fe, ^{72}Ga, ^{76}As, ^{82}Br, ^{122}Sb, ^{181}Hf, ^{182}Ta, ^{187}W, ^{239}Np, ^{95}Zr, ^{99}Mo, ^{103}Ru, ^{131}I, ^{132}Te, ^{132}I, ^{133}I, ^{138}Cs, ^{140}Ba, ^{140}La and ^{147}Nd, and natural-series nuclides (^{212}Pb, ^{208}Tl, ^{214}Pb, ^{214}Bi, ^{228}Ac). Lines with emission probability of at least 0.5% between 40 and 3000 keV are retained, and only nuclides with two or more such lines are kept, since a single-line nuclide carries no information on density.

A library line matches a peak if the energies agree within the larger of 0.6 keV and half the FWHM. Expected relative areas for each nuclide are computed from the emission probabilities and the nominal efficiency and scaled to the matched peaks. A line counts as missing if its expected area exceeds three times the Currie detection limit $L_D = 2.71 + 4.65\sqrt{B}$ [19], with the continuum B estimated from side bands two to three FWHM away. The factor of three leaves room for the fact that the nominal efficiency over-predicts low-energy lines in a dense sample. A nuclide is accepted when at least two lines match, its strongest expected line is among them, and the matched lines carry at least 60% of the expected counts once missing lines are counted against it. Peaks claimed by more than one accepted line are flagged as interfered and excluded from the density fit by default, as are lines outside the energy range of the surface and lines with area less than five times its uncertainty.

Output and testing

The code writes tables of peaks, nuclides, lines, line-pair densities, the corrected efficiency curve with its uncertainty band, the two-dimensional efficiency grid $\varepsilon(E, \rho)$ and activities, along with a text summary and figures. Users with their own MCNP results for a different detector or geometry can fit a new surface of the same form from a table of density, energy and efficiency and load it in place of the default surface.

Testing used synthetic spectra, because no measured spectra of dense, well-characterized multi-gamma samples were available for this study. The generator places each line at the expected area $a\,I\,\varepsilon_{true}(E, \rho)\,t_{live}/C_d$, where ε_{true} follows Eq. 3 with a chosen surface and an optional energy-dependent detector factor. A suite of 15 automated tests, all passing, checks among other things that the surface reproduces the published coefficient listing, that pair densities round-trip, that peak areas are unbiased, that density is recovered across the range, that uncertainties have the expected coverage and that the graphical interface runs end to end.

Results and discussion

Demonstration spectrum

The demonstration case is a 7200 s synthetic spectrum of a sample with a density of 8 g cm^{-3} containing ^{152}Eu (6000 Bq), ^{133}Ba (4000 Bq), ^{60}Co (3000 Bq) and ^{24}Na (4000 Bq), analyzed with ρ_{cal} = 1 g cm^{-3} and the surface itself as nominal efficiency. Figure 1 shows the efficiency surface of Eq. 3 with the fitted density marked on it, and Figure 2 shows the spectrum. The search found 28 peaks. Four nuclides were accepted and 23 of their lines passed the selection criteria and entered the fit.

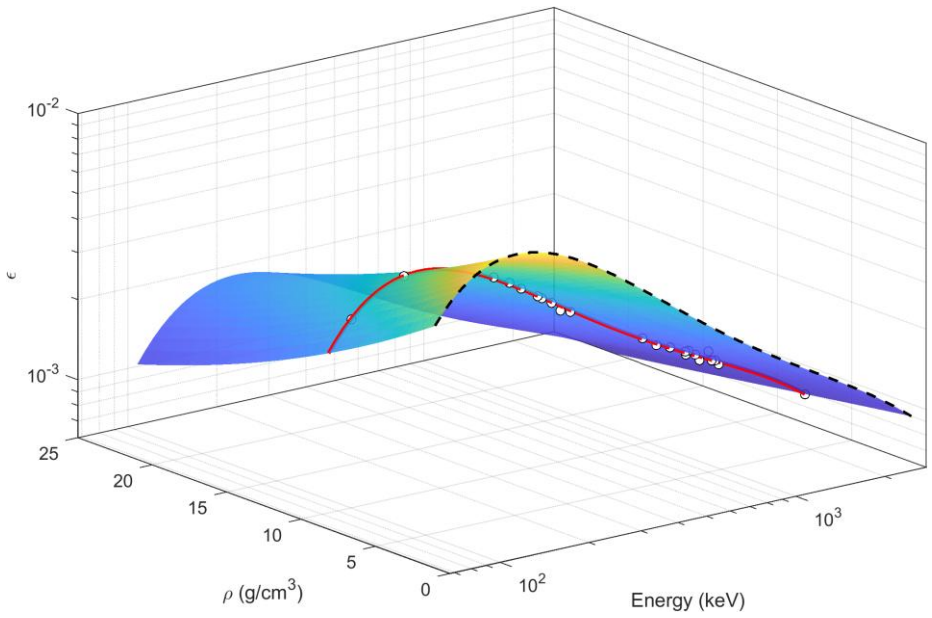


Fig. 1 Two-dimensional full-energy peak efficiency $\varepsilon(E, \rho)$ from Eq. 3 with ρ_{cal} = 1 g cm^{-3}. The dashed curve is the nominal efficiency at ρ_{cal}. The solid red curve is the efficiency at 8.15 g cm^{-3} calculated by SSEff as the efficiency. The circles are the efficiencies of the 23 lines used in the fit

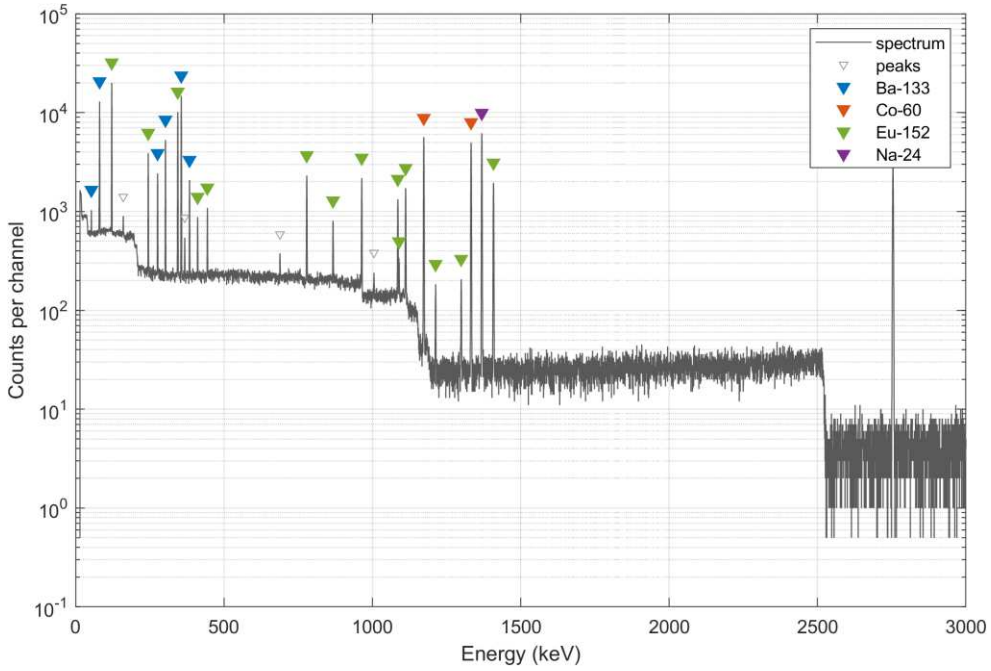


Fig. 2 Synthetic 7200 s spectrum of the demonstration sample (density 8 g cm^{-3}). Filled markers show peaks assigned to ^{133}Ba, ^{60}Co, ^{152}Eu and ^{24}Na. Open markers show peaks that were found but not assigned due to their being below the threshold.

The SSEff fit gave ρ_{eff} = 8.15 ± 0.63 g cm^{-3}. Figure 3 shows the calculated efficiency curve after each nuclide has been scaled by its fitted c_n. The points from four different nuclides fall on one curve, and that curve lies well below the nominal calibration (dashed line). The corrected efficiency, which includes the density uncertainty, is 4.4% at 122 keV and 2.4% at 2614 keV.

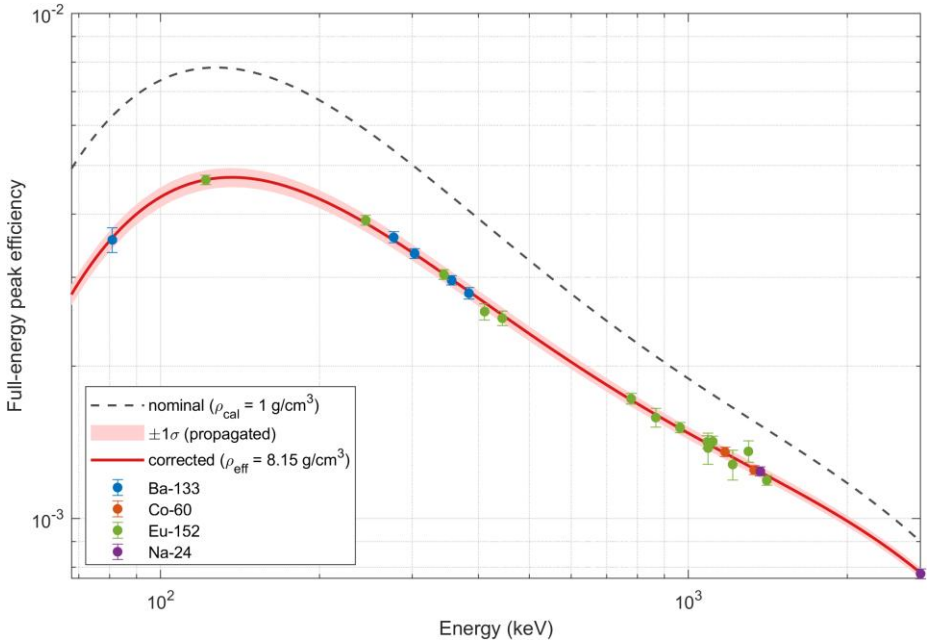


Fig. 3 Calculated efficiencies of the demonstration sample. The dashed line is the nominal efficiency (ρ_{cal} = 1 g/cm^3) and the red solid line is corrected efficiency at ρ_{eff} = 8.15 g/cm^{-3}.

Table 1 compares the activities and illustrates the need for the self-shielding correction. The nominal result for ^{60}Co is instructive as its two lines are close in energy that they agree with each other even though both are 20% low. Accordingly a a consistency check on a single close pair would not have revealed the problem. This illustrates the benefit of having radionuclides in the spectrum with multiple gamma-rays lines over a wide range of energies.

Table 1 Weighted-mean activities (Bq) of the demonstration sample with the nominal efficiency and with the self-shielding corrected efficiency (ρ_{eff} = 8.15 g cm^{-3}). Uncertainties are one standard deviation with corrected uncertainties including the density uncertainty.

Nuclide	True	Nominal	Corrected
^{133}Ba	4000	2706 ± 31	4024 ± 135
^{60}Co	3000	2412 ± 36	3015 ± 72
^{152}Eu	6000	4301 ± 33	6033 ± 165
^{24}Na	4000	3341 ± 50	4001 ± 86

Which line pairs carry the information

The two-line method can be applied to each of the 103 line pairs available in the demonstration spectrum. Of these, 82 have a root inside the density range, and their median is 7.87 g cm^{-3}. Figure 4 shows that the individual results are very uneven. Pairs with energies close together scatter from 1 to beyond 20 g cm^{-3} with uncertainties to match while pairs spanning a wide energy range cluster around the true value. The best single pair is ^{152}Eu with gamma-ray lines at 121.8 and 1408.0 keV. Utilization of this line pair results in a calculated sample density of 7.56 ± 0.87 g cm^{-3}.

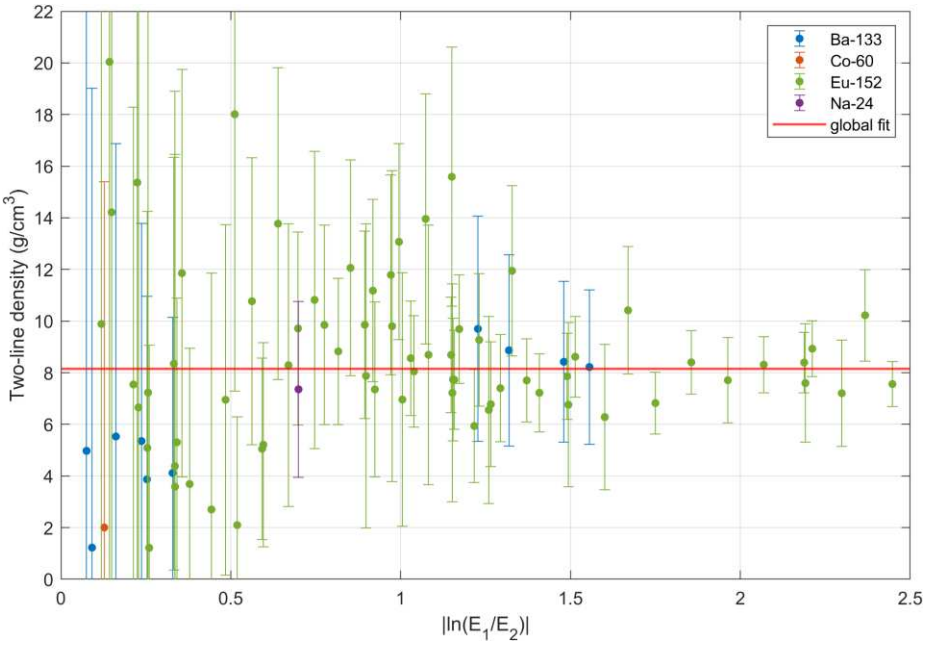


Fig. 4 Two-line densities (Eq. 5) for every line pair in the demonstration spectrum, plotted against the energy separation

Equation 6 makes this quantitative. At 8 g cm^{-3}, with a 2% standard uncertainty on each of the two apparent efficiencies, the sensitivity of the ^{152}Eu 121.8 and 1408.0 keV pair is −0.035 per g cm^{-3} resulting in a density uncertainty of 0.81 g/cm^3. In contrast, the ^{24}Na 1368.6 and 2754.0 keV pair results in a density of 3.3 g cm^{-3} and the ^{60}Co pair at 1173.2 and 1332.5 keV results in a calculated density of 16 g cm^{-3}. The best line pairs for the density calculation results from line pairs that have a wide energy spans and a line below a few hundred keV. This has a practical consequence for debris analysis: ^{24}Na, ^{56}Mn and ^{60}Co are often the strongest multi-line activation products but nuclides such as ^{152}Eu, ^{133}Ba, ^{182}Ta or ^{239}Np provide strong lines on both sides of 300 keV that provide more accurate density estimates.

Validation over the density range

Five synthetic spectra with different random seeds were analyzed at each of eight densities between 1.5 and 20 g cm^{-3} with the same nuclides and activities as the demonstration case. Table 2 and Fig. 5a summarize the results. The mean fitted density is within 0.3 g cm^{-3} of the true value over the entire range with no trend in the bias. The

typical density uncertainty grows from 0.43 g cm^{-3} at 1.5 g cm^{-3} to about 1.0 g cm^{-3} at 17–20 g cm^{-3}.

Table 2 Density recovered from synthetic spectra (five per density). $\bar{\sigma}$ is the mean reported uncertainty. The last column is the mean bias of activities computed with the nominal efficiency.

True ρ (g/cm^3)	Mean fitted ρ (g/cm^3)	SD of fits (g cm^{-3})	$\bar{\sigma}$ (g/cm^{-3})	Nominal activity bias (%)
1.5	1.58	0.16	0.43	−2.4
3	2.99	0.15	0.47	−7.8
5	5.10	0.27	0.53	−15.2
8	7.87	0.32	0.61	−23.7
11	10.93	0.17	0.73	−31.6
14	14.27	0.56	0.88	−39.0
17	16.74	0.67	1.02	−43.7
20	20.13	0.38	1.03	−49.3

Nuclides and activities as in Table 1; analysis with the 2% surface-model uncertainty of Eq. 9

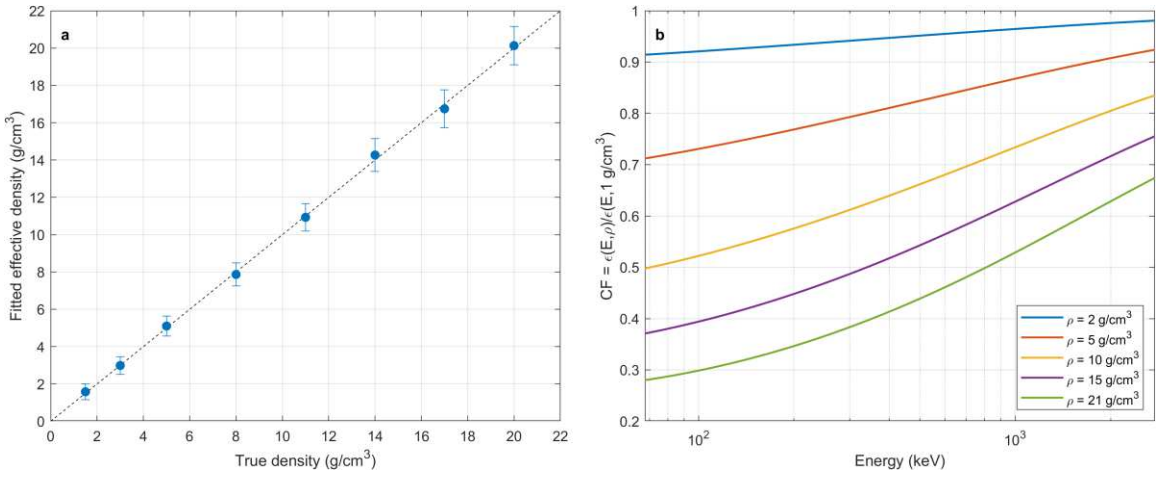


Fig. 5 a Effective density fitted to synthetic spectra (five per density) versus the true density; the dashed line is the identity. **b** Self-shielding correction factor of Eq. 4 relative to ρ_{cal} = 1 g cm^{-3} for densities from 2 to 21 g cm^{-3}.

The spread of the fits is smaller than the reported uncertainty, by a factor of 1.5 to 4. This is the expected effect of the 2% model term which is present in the weights but absent from synthetic data drawn from the same surface.

Limitations

The most important limitation is that all quantitative validation here uses synthetic spectra generated from the efficiency surfaces themselves. The tests show that the code is internally consistent, that the fit is unbiased and its uncertainties are realistic when the model is right, and that the hybrid form tolerates a wrong detector model. They do not show that the surface describes real dense samples. That requires measured spectra of multi-gamma sources dispersed in matrices of known density in the modeled geometry, and such measurements are the obvious next step.

The surface is for a carbon matrix (Z = 6). The effective density returned by SSEff is therefore the density of a carbon-equivalent sample of the same size and shape that would produce the same energy dependence of attenuation. For low-Z materials such as concrete, glass and soil this is a reasonable description above about 100 keV, where Compton scattering dominates, but for matrices containing lead, iron or actinides the photoelectric contribution and K-edges change the shape of the correction at low energy [2]. For such samples the low-energy lines should be removed from the fit. Inhomogeneous samples, such as a dense inclusion in a light matrix, are described by an average density at best.

True-coincidence summing is not modeled in the surface or in the analysis. At 12 cm the effect is small, but for cascade emitters such as ^{60}Co, ^{152}Eu and ^{133}Ba counted close to the detector it would bias line ratios and therefore density, and it should be corrected before the density fit. Dead-time and pile-up effects in high-activity samples are likewise outside the model. Finally, the surface should not be extrapolated beyond 67.75–2754 keV or 1–21 g cm^{-3}. Lines outside the energy range are excluded automatically and densities are confined to the range.

Conclusions

An MCNP efficiency surface, combined with line ratios of single nuclides that determine sample density, provides a self-attenuation correction that needs no transmission measurement and no knowledge of the activity. The method described here keeps the laboratory's measured calibration and applies only the density dependence of the surface. To achive this SSEff fits all lines of all identified multi-gamma nuclides at once and propagates the uncertainties of the peak areas. Testing of this method showed that the density was properly calculated within 0.3 g cm^{-3} over a range of sample densities from 1.5 to 20 g cm^{-3}. Calculated corrected activities were within 1% of the modeled activity in the demonstration case. Corrections due to self-shielding ranged from 16% to 32%. The analysis of line pairs shows that wide energy spans with a low-energy line are the most valuable for these calculations. Nuclides such as ^{152}Eu, ^{133}Ba or ^{182}Ta significantly aid in the ability to calculate sample density. The MATLAB code, SSEff, carries out the full analysis from a spectrum or peak list to a corrected efficiency curve and activities. Validation with measured spectra of dense, characterized samples, and surfaces for higher-*Z* matrices, are the work that remains.

Acknowledgements

The MCNP modeling underlying the efficiency surface was supported by the Defense Threat Reduction Agency under award number HDTRA1-16-1-0037.

Declarations

Conflict of interest

The author declares no conflict of interest.

References

1. Vieira BJ, Biegalski SR, Freitas MC, Landsberger S (2006) Atmospheric trace metal characterization in industrial area of Lisbon, Portugal. J Radioanal Nucl Chem 270:55–62. https://doi.org/10.1007/s10967-006-0309-0
2. Knoll GF (2010) Radiation detection and measurement, 4th edn. Wiley.
3. Gilmore G (2008) Practical gamma-ray spectrometry, 2nd edn. Wiley, Chichester, UK.
4. Cutshall NH, Larsen IL, Olsen CR (1983) Direct analysis of ^{210}Pb in sediment samples: self-absorption corrections. Nucl Instrum Methods Phys Res 206:309–312. https://doi.org/10.1016/0167-5087(83)91273-5
5. Jodłowski P (2016) A revision factor to the Cutshall self-attenuation correction in ^{210}Pb gamma-spectrometry measurements. Appl Radiat Isot 109:566–569. https://doi.org/10.1016/j.apradiso.2015.11.092
6. Glasstone S, Dolan PJ (1977) The effects of nuclear weapons, 3rd edn. US Department of Defense and US Department of Energy, Washington, DC
7. National Research Council (2010) Nuclear forensics: a capability at risk (abbreviated version). National Academies Press, Washington, DC. https://doi.org/10.17226/12966
8. Burnett JL, Milbrath BD (2016) Radionuclide observables for the Platte underground nuclear explosive test on 14 April 1962. J Environ Radioact 164:232–238. https://doi.org/10.1016/j.jenvrad.2016.08.002
9. Biegalski S, Kane N, Mann J, Tipping T, Dayman K (2018) Neutron activation of NIST surrogate post-detonation urban debris (SPUD) candidate SRMs. J Radioanal Nucl Chem 318:187–193. https://doi.org/10.1007/s10967-018-6023-x
10. Aghara S, Charlton W (2006) Characterization and quantification of an in-core neutron irradiation facility at a TRIGA II research reactor. Nucl Instrum Methods Phys Res B 248:181–190. https://doi.org/10.1016/j.nimb.2006.04.074
11. Graham J, Landsberger S, Ferreira PJ, Ihlefeld J, Brennecka G (2012) Neutron flux characterization techniques for radiation effects studies. J Radioanal Nucl Chem 291:503–507. https://doi.org/10.1007/s10967-011-1270-0
12. Kane NL (2019) Analysis of surrogate post-detonation urban debris (SPUD) gamma rays and self-attenuation. MS Thesis, Georgia Institute of Technology, Atlanta, GA
13. Goorley T et al (2012) Initial MCNP6 release overview. Nucl Technol 180:298–315. https://doi.org/10.13182/NT11-135

14. Lewis EE, Miller WF Jr (1993) Computational methods of neutron transport. American Nuclear Society, La Grange Park, IL.
15. Canberra Industries (2016) Genie 2000 gamma acquisition and analysis, V3.4.1 (software). Canberra Industries, Meriden, CT.
16. Birge RT (1932) The calculation of errors by the method of least squares. Phys Rev 40:207–227. https://doi.org/10.1103/PhysRev.40.207
17. Mariscotti MA (1967) A method for automatic identification of peaks in the presence of background and its application to spectrum analysis. Nucl Instrum Methods 50:309–320. https://doi.org/10.1016/0029-554X(67)90058-4
18. National Nuclear Data Center (2026) NuDat 3.0. Brookhaven National Laboratory, Upton, NY. https://www.nndc.bnl.gov/nudat3/.
19. Currie LA (1968) Limits for qualitative detection and quantitative determination. Application to radiochemistry. Anal Chem 40:586–593. https://doi.org/10.1021/ac60259a007